

Study of nanoscale magnetic structures fabricated using electron-beam lithography and quantum magnetic disk

Stephen Y. Chou, Mark Wei, Peter R. Krauss, and Paul B. Fischer

Department of Electrical Engineering, University of Minnesota, Minneapolis, Minnesota 55455

(Received 22 June 1994; accepted 31 August 1994)

Two types of nanoscale single-domain magnetic structures were fabricated using e-beam nanolithography and were studied using magnetic force microscopy. The first structure is the isolated and interactive arrays of Ni bars on silicon that are 35 nm thick, 1 μm long, and have widths ranging from 15 to 200 nm and spacings ranging from 200 to 600 nm. The second structure is an array of Ni pillars on silicon that have a uniform diameter of 35 nm, a height of 120 nm, and a density of 65 Gbits/in²—over two orders of magnitude greater than the state-of-the-art magnetic storage density. It was found that the magnetic properties of these structures can be controlled by engineering their size and spacing. When the bar width is smaller than 150 nm, the bars become single magnetic domain. As the width of the isolated bars decreased from 200 to 55 nm, the magnetic field needed to switch the magnetization of these bars increased monotonically from 100 to 740 Oe which is the highest field reported for Ni. However, further reduction of bar width led the switching field to decrease due to thermal effect. Furthermore, it was found that as the bar spacings become smaller, the interaction between the bars will reduce the switching field. Finally, based on the artificially patterned single-domain magnetic structures, we propose a new paradigm for ultra-high-density magnetic recording media: quantum magnetic disk.

I. INTRODUCTION

Coercivity, coercive squareness, and many other magnetic properties of a magnetic thin film strongly depend upon the geometric factors of the magnetic grains in the film such as the grain size and anisotropy, the grain magnetization orientation, and the spacing between the grains. Generally, however, in a conventional as-deposited magnetic film the magnetic grains have a broad distribution of the grain size, anisotropy, spacing, and nearly random magnetization. Therefore the conventional magnetic media have a large variation of local magnetic properties, making them unsuitable for ultra-high-density recording and hard to compare with theory. To develop new materials for ultrahigh magnetic recording and to obtain a better understanding of magnetic behavior of a material, many methods have been attempted in order to control the geometric factors of magnetic grains in a thin film. The approaches include control of film deposition conditions, alloying, epitaxial growth on crystal substrates, introduction of stacking faults, and insertion of non-magnetic material between the magnetic grains. However, none of these approaches offers precise control of the geometric factors.

As nanofabrication technology advances, it is now possible to precisely control the geometrical factors of magnetic grains in a thin film using nanolithography. These nanolithographically defined magnetic materials open up new opportunities to engineer novel magnetic materials and understand the fundamentals of magnetism. Recently, a joint team from the University of California at San Diego and IBM studied nanoscale permalloy bars fabricated using electron-beam lithography.^{1,2} In that study, isolated bars had a fixed length of 1 μm and a fixed width of 133 nm; interactive bar arrays had a fixed spacing with the strongest coupling along the bars' long axis.

In this article, we present the investigation of isolated Ni bars with a width varying from 15 to 200 nm, and interactive Ni bar arrays with a spacing varying from 200 to 600 nm with the strongest coupling in the bars' short axis. We will report the effects of bar width and spacing on the switching field of these isolated and interactive bars. We will also report the study of arrays of Ni pillars that have a uniform diameter of 35 nm, a height of 120 nm, and a density of 65 Gbits/in²—over two orders of magnitude greater than the state-of-the-art magnetic storage density. Furthermore, we will discuss a new paradigm for ultra-high-density magnetic recording based on the lithographically defined nanomagnetic structures.

II. ULTRA-HIGH-DENSITY NANOMAGNETIC BAR ARRAYS AND PILLAR ARRAYS

The isolated and interactive nanomagnetic nickel bars were fabricated using electron-beam nanolithography and a lift-off process.³ All the bars are 35 nm thick. For isolated bars, the bar length was fixed at 1 μm , the spacing between bars was 10 μm , but the bar width varied from 15 to 200 nm. Figure 1 shows a scanning electron micrograph of a Ni bar with a 15 nm width and an average edge variation of 4 nm. For interactive bar arrays, the bar width and length were fixed at 100 nm and 1 μm , respectively. The spacing between bars along the long axis was 2 μm , but the spacing between the bars along the short axis varied from 200 to 600 nm. Therefore the interaction between bars is primarily along the short axis, and the bar arrays can be regarded as isolated rows of one-dimensional interactive arrays. This is very different from that in Ref. 1 where the bars were coupled primarily along the long axis. To illustrate the fabrication precision and uniformity, Fig. 2 shows a large array of Ni bars

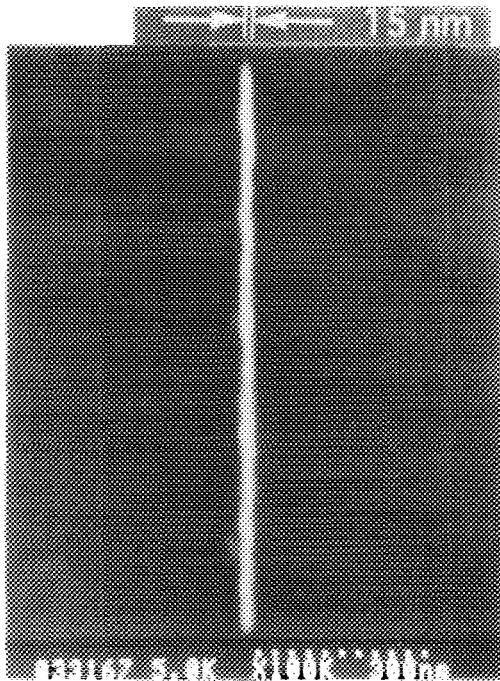


FIG. 1. SEM image of a high aspect ratio isolated Ni bar that is $1\ \mu\text{m}$ long and $15\ \text{nm}$ wide.

which are $20\ \text{nm}$ wide, $200\ \text{nm}$ long, and $150\ \text{nm}$ apart along the short axis and $100\ \text{nm}$ apart along the long axis.

To study the vertical magnetic recording, arrays of Ni pillars on silicon were fabricated using electron-beam nanolithography and electroplating. The details of the fabrication

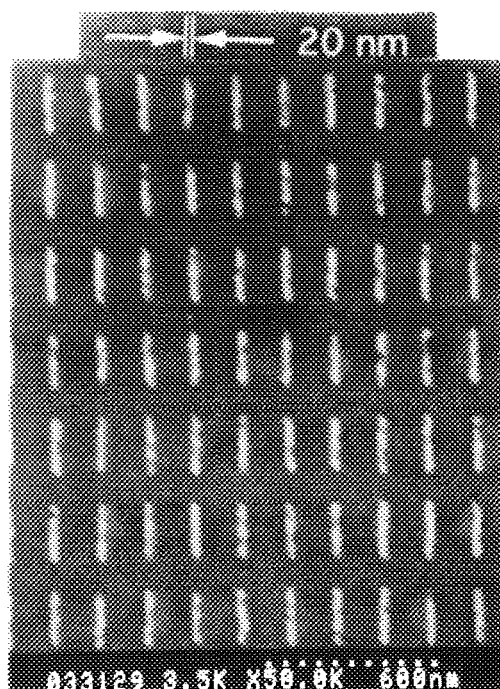


FIG. 2. SEM image of interactive bar arrays. Each bar is $20\ \text{nm}$ wide, $200\ \text{nm}$ long, and $35\ \text{nm}$ thick. The spacings are 130 and $100\ \text{nm}$ in the short and long axes, respectively.

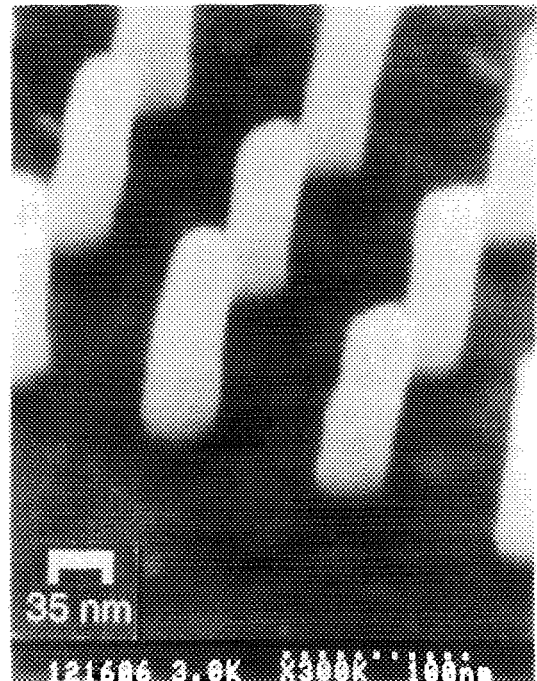


FIG. 3. SEM image of Ni pillar array of $35\ \text{nm}$ diameter, $120\ \text{nm}$ height, and a $100\ \text{nm}$ spacing. The density is $65\ \text{Gbits/in.}^2$ and the aspect ratio is 3.4 .

are reported elsewhere.⁴ As shown in Fig. 3, the pillars have a uniform diameter of $35\ \text{nm}$, a height of $120\ \text{nm}$, and a period of $100\ \text{nm}$; therefore the density of the pillar arrays is $65\ \text{Gbits/in.}^2$ —over two orders of magnitude greater than the state-of-the-art magnetic storage density.

III. MAGNETIC PROPERTIES

The nanomagnetic bars were studied using a custom built magnetic force microscope (MFM) that was modified from a commercial atomic force microscope (AFM). The MFM was operated in amplitude detection mode at $\sim 300\ \text{mTorr}$ vacuum for a high sensitivity. The MFM tips are the ordinary AFM cantilevers coated with $30\ \text{nm}$ of cobalt and have a resonance frequency of $18\ \text{kHz}$. These soft tips give better sensitivity, but poorer resolution, than that of a harder tip.

Before the isolated bars were put into any magnetic field, MFM images of the sample were taken. These images showed that for bars of a width smaller than $150\ \text{nm}$, the virgin magnetic state is single domain with magnetization along the direction of its easy (i.e., long) axis, and the bars of wider width are multidomain.

In measuring the switching field of the isolated bars, the sample was first saturated in a fixed direction along its easy axis using a $2000\ \text{Oe}$ magnetic field, and an MFM image was taken to determine its magnetization. Then a test field was applied in the opposite direction and returned to zero. The sample was examined under MFM again to see if its magnetization flipped. If the bar flipped, a smaller test field was applied in the next measuring cycle; otherwise, a larger field was applied. This process continued until the switching field of a nickel bar was located within $10\ \text{Oe}$.

It was found that the magnetization switching field of an isolated bar is a strong function of width, as shown in Fig. 4.

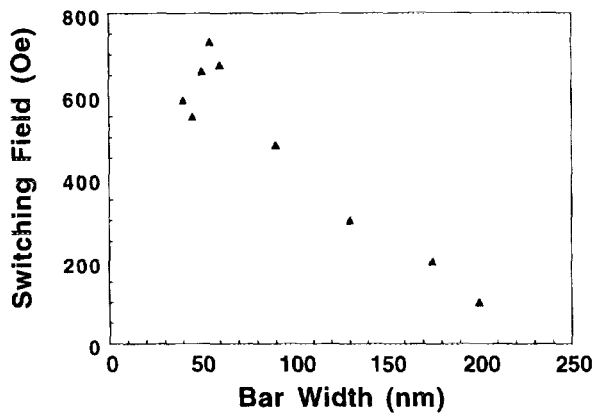


FIG. 4. Switching field of isolated bars vs bar width. The maximum switching field is 740 Oe for 55 nm wide bars. The bars are 1 μm long and the bar width was the actual size measured using SEM.

As the bar width decreases from 200 to 55 nm, the switching field increases from 100 to 740 Oe, which is, to our best knowledge, the highest switching field reported for Ni. This field is about 30 times larger than the coercivity of the Ni film that was evaporated at the same time during the bar's fabrication. The increase in switching field is due to the fact that a narrower width will have a larger anisotropy and generally require a larger energy to switch. However, as the bar width decreases further, the switching field starts decreasing due to the fact that thermal energy becomes comparable to magnetization switching energy.

The interactive bar arrays have a bar width of 100 nm and a spacing between bars of 0.2, 0.4, and 0.6 μm , respectively along the short axis. Figure 5 shows a MFM image of these bar arrays. The bright spot represents the north pole and the dark spot represents the south pole and the

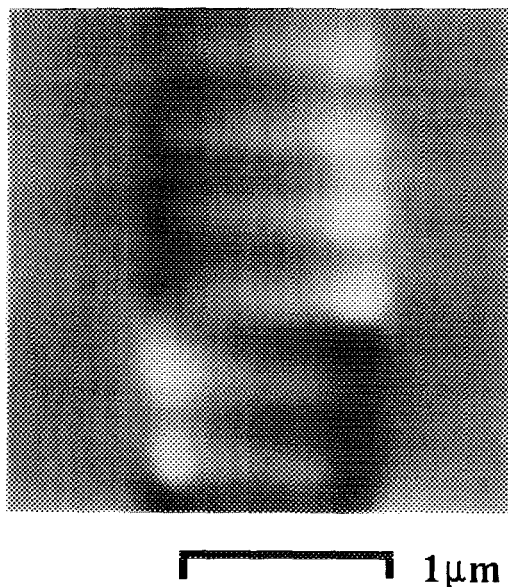


FIG. 5. MFM image of one-dimensional interactive bar arrays with 400 nm spacing, 1 μm bar length, and 100 nm bar width. The bright spot represents the north pole and the dark spot represents the south pole.

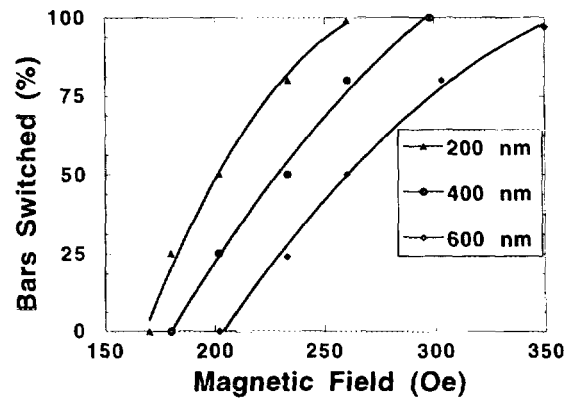


FIG. 6. Percentage of bars that switched vs the applied magnetic field for interactive bars with a spacing along the short axis of 200, 400, and 600 nm.

dark spot represents the south pole. The switching field versus the bar spacing was measured and is shown in Fig. 6. In this measurement, an average of about 30 bars were counted for each data point and the bars at the end of each row were not counted. Figure 6 shows three facts. First, smaller spacing results in a smaller switching field. The switching field for a 100 nm wide isolated bar is 300 Oe. But due to interaction, the mean value of the switching field (i.e., the field at which 50% of bars can flip) is 205, 232, and 260 Oe for a spacing of 0.2, 0.4, and 0.6 μm , respectively. Second, the switching field decreases almost linearly with the reduction of spacing at a rate 15 Oe per 100 nm. This behavior is due to the fact that as the spacing decreases, the demagnetization field generated by neighboring bars increases and will help a bar to flip. Third, the switching field has a distribution about 100 Oe which is due to bar interaction as well as size variations.

We also have attempted to use a high-resolution MFM to examine ultra-high-density pillar arrays, but were unsuccessful. The primary reason is that since the topology image and magnetic image are intertwined in MFM, the aspect ratio of our nanomagnetic pillars is so large that the topology image completely masks the magnetic image. Despite the difficulty in characterizing these nanomagnetic pillars, MFM measurements showed that horizontal nanomagnetic bars of 35 nm thickness and nanoscale widths that were plated using the same technology are single domain, consistent with our theoretical estimation that the nanomagnetic pillars should be single domain as well.⁵

Finally, it should be pointed out that the simulations that are based on current magnetic switching models cannot match experimental data.⁶ Therefore the experimental study is providing the benchmark as well as insight into developing better magnetic models and simulation tools.

IV. QUANTUM MAGNETIC DISK

Based on these artificially patterned single-domain magnetic structures, we propose a new paradigm for ultra-high-density magnetic disk: quantum magnetic disk (QMD).⁷ As shown in Fig. 7, a quantum magnetic disk consists of prepatterned single-domain magnetic structures embedded uni-

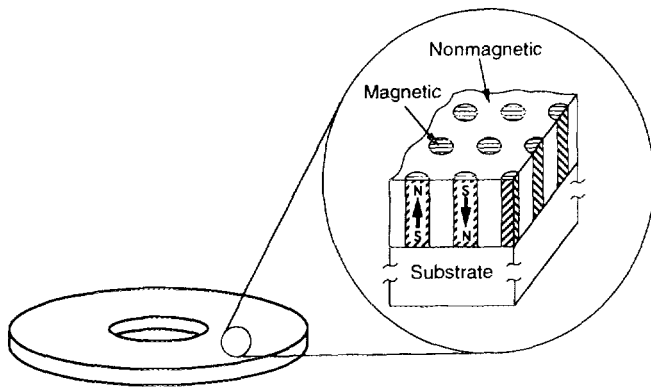


FIG. 7. Schematic of a quantum magnetic disk which consists of prepatterned single-domain magnetic structures embedded in a nonmagnetic disk. Only the vertical magnetization is shown, but the disk can be made with longitudinal magnetization.

formly in a nonmagnetic disk. Each bit in the quantum magnetic disk is represented by a prefabricated single-domain magnetic structure that has a uniform and well-defined shape, a prespecified location, and, the most importantly, a quantified magnetization that has only two states: the same in value and opposite in direction. In other words, the shape, magnetization, and location for each bit in a quantum magnetic disk are all quantized and predefined during the disk manufacturing. On the contrary, in a conventional magnetic disk where a bit is not defined at disk fabrication, the shape and magnetization of each bit have a broad distribution and the location of a bit can be anywhere on disk. The QMD also differs from discrete track disk^{8,9} and discrete segment disk^{10,11} where the magnetization (both value and direction) of each bit can have a continuous and broad distribution.

The advantages of quantum magnetic disks over the conventional disks are apparent. First, the writing process in the quantum disk is greatly simplified, resulting in much lower noise and less error rate and allowing much higher density. In the quantum disk, the writing process does not define the location, shape, and magnetization value of a bit, but just simply flips the quantized magnetization orientation of a prepatterned single-domain magnetic structure. The writing can be perfect, even though the head slightly deviates from the intended bit location and partially overlaps with other bits, as long as the head flips only the magnetization of the intended bit. But in the conventional magnetic disk, the writing process must define the location, shape, and magnetization of a bit. If the head deviates from the intended location, the head will write part of the intended bit and part of its neighboring bits.

Second, the quantum disk can track every bit individually, but the conventional disk cannot track all of its bits. This is

because that in quantum disk, each bit is separated from others by nonmagnetic material, but in the conventional disk, many bits are connected. The individual-bit-tracking ability allows precise positioning, less error rate, and therefore ultra-high-density storage.

Finally, reading in the quantum disk has much less jitter than that in the conventional disk. The reason is that in conventional disk the boundary between bits is ragged and not well defined, but in the quantum disk, each bit is defined with nanometer precision (can be much less than the grain size) and is well separated from each other.

V. CONCLUSION

Isolated and interactive arrays of Ni bars that are 35 nm thick, 1 μm long, and have widths ranging from 15 to 200 nm and spacing ranging from 25 nm to 2 μm , and arrays of Ni pillars on silicon that have a uniform diameter of 35 nm, a height of 120 nm, and a density of 65 Gbits/in.² were fabricated using e-beam lithography and were studied with magnetic force microscopy. It was found that the magnetic properties of the lithographically defined structures can be engineered by precise control of the structure's geometric factors. It was found that bars with a width smaller than 150 nm and the pillars are single magnetic domain. It was also found that as the width of the isolated bars decreased from 200 to 55 nm, the magnetic field for switching the magnetic moment of these bars increased monotonically from 100 to 740 Oe—the highest reported. However, further reduction of the bar width led the switching field to decrease due to thermal effects, then to increase. Furthermore, it was found that the interaction between the bars will reduce the switching field. Finally, based on the artificially patterned single-domain magnetic structures, a new paradigm for ultra-high-density magnetic recording media, the quantum magnetic disk is proposed.

ACKNOWLEDGMENTS

The authors would like to thank J. G. Zhu for stimulating discussion, Hao Fang for MFM measurements, and Bob Guibord for this technical assistance in fabrication. This work was supported in part by ARPA and ONR.

¹J. F. Smyth, S. Schultz, D. R. Fredkin, T. Koehler, I. R. McFaydin, D. P. Kern, and S. A. Rishton, *J. Appl. Phys.* **63**, 4237 (1988).

²G. A. Gibson, J. F. Smith, S. Schultz, and D. P. Kern, *IEEE Trans. Magn.* **MAG-27**, 5187 (1991).

³S. Y. Chou and P. Fischer, *J. Vac. Sci. Technol. B* **8**, 1919 (1990).

⁴P. R. Krauss and S. Y. Chou, *J. Vac. Sci. Technol. B* **12**, 3639 (1994).

⁵A. Aharioni, *J. Appl. Phys.* **63**, 5879 (1988).

⁶J. G. Zhu and J. Gadbois (private communication).

⁷S. Y. Chou (private communication).

⁸L. F. Shew, *IEEE Trans. Broadcast Telev. Receivers* **BTR-9**, 56 (1963).

⁹S. E. Lambert, I. L. Sander, A. M. Patlach, and M. T. Krounbi, *IEEE Trans. Magn.* **MAG-23**, 3690 (1987).

¹⁰K. A. Belsler, T. Makansi, and I. L. Sanders, US Patent No. 4,912,585 (27 March, 1990).

¹¹S. E. Lamber, I. L. Sanders, A. M. Pattan, M. T. Krounbi, and S. R. Hetzler, *J. Appl. Phys.* **69**, 4724 (1991).